Cryst. Res. Technol. **43**, No. 10, 1041 – 1045 (2008) / **DOI** 10.1002/crat.200800109

Morphology and photoluminescence properties of ZnO nanostructures fabricated with different given time of Ar

D. D. Wang[1,2], J. H. Yang*[3,1,2], L. L. Yang[3], Y. J. Zhang[3], J. H. Lang[3], and M. Gao[3]

[1] Key Laboratory of Excited State Processes, Changchun Institute of Optics, Fine Mechanics and Physics, Chinese Academy of Sciences, Changchun, 130033, P. R. China
[2] Graduate School of the Chinese Academy of Sciences, Beijing, 100049, P. R. China
[3] The Institute of Condensed Matter Physics, Jilin Normal University, Siping, 136000, P. R. China

Received 14 April 2008, revised 26 May 2008, accepted 9 June 2008
Published online 4 July 2008

Key words II-VI semiconductors, photoluminescence, thermal carbon reduction.
PACS 71.55.Gs, 78.55.-m

ZnO nanostructures were grown on Au-coated Si (100) substrates by carbonthermal reduction method with the help of Ar at the beginning of growth. The structural and optical properties of ZnO nanostructures strongly depended on the supply time of Ar. When the given time of Ar gas current was 90s, sample was ZnO nanowires with hexagonal morphology. The Raman spectroscopy revealed the low level of oxygen vacancies and Zn interstitials in samples. Room temperature photoluminescence (PL) spectra exhibited the intensity of green emission increased on the condition of rich oxygen (decrease given time of Ar) and the nanowire had strongest intensity of UV emission compared with other nanostructures. Green emission is ascribed to the electron transition from the bottom of the conduction band to the antisite defect O_{Zn} level.

1 Introduction

As a wide band gap (3.37 eV at room temperature) semiconductor with large exciton binding energy of 60 meV, ZnO is a promising material for electronic and optical devices [1-8]. In recent years, one–dimensional (1D) ZnO nanostructures have attracted extraordinary attention for their potential applications in device and interconnect integration in nanoelectronics and molecular electronics [9-12]. So far, synthesis of 1D ZnO nanostructures has widely been reported [1-6]. Yang et al. made a ZnO nanowire array for ultraviolet laser and a dendritic nanowire for ultraviolet laser array [5-6]. Wang et al. [8] reported on single-crystal nanobelts [1], nanorings [3] and bicrystalline ZnO nanowires. However, there are some problems of growth and optical properties that need further study. On one hand, most ZnO nanowires have been mainly grown on sapphire substrates [13-17] by metal organic chemical vapor deposition (MOCVD) and metal organic vapor phase epitaxy (MOVPE) and so on. These methods involved complex procedures and sophisticated equipments. Moreover the sapphire substrates are rare, expensive and difficult to integrate. On the other hand, intrinsic ZnO has been observed to emit radiation in the UV and green spectral region. The origin of the green luminescence is still in dispute.

In this paper, with the help of Ar at the beginning of growth, ZnO nanostructures were synthesized on Au-coated Si (100) substrates by carbonthermal reduction method. The effects of Ar supply time on the morphologies, and optical properties of ZnO nanostructures were investigated systematically. The origin of the green luminescence of samples was also discussed in detail.

2 Experimental

Figure 1 is the sketch map of the growth equipment. A mixture of ZnO (99.99%, 325 mesh, Alfa Aesar) powder and carbon (99.99%, 325 mesh, Alfa Aesar) powder with a 1:1 mass ratio was placed in a quartz boat.

* Corresponding author: e-mail: jhyang1@jlnu.edu.cn

Au-coated Si substrate covered the boat and upend above the mixture. The quartz boat was put into a small quartz tube. When the temperature of the furnace was 850°C, the quartz tube was placed inside a horizontal tube furnace. The Ar gas was supplied into the furnace for different time. After suppling the Ar gas, two air valves were closed to keep the furnace obturation as shown in figure 1. The temperature was synchronously ramped to 900°C rapidly and kept for 1 h. After the furnace was cooled to room temperature, light or dark gray product was found on the substrate. Three samples labeled as a, b and c were synthesized with different supply time of the Ar, which is corresponding to 30, 90 and 180 s, respectively. In the process, due to Si substrate was above the mixture, the Ar just adjusted to the ambient gas composition in the furnace, which was differernt from the vapor phase transport process [8].

SEM (Hitachi, S-570), XRD (MAC Science, MXP18, Japan), Raman (LABRAM-UV, Jobin Yvon, France) and PL (LABRAM-UV, Jobin Yvon, France) were used to characterize the surface morphology, crystal structure and optical properties of the ZnO nanostructures.

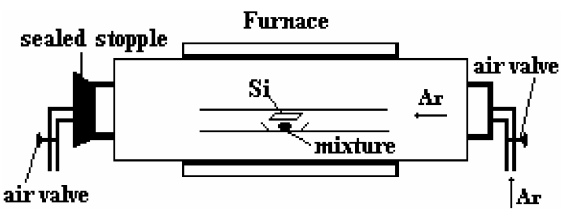

Fig. 1 Sketch map of the growth equipment.

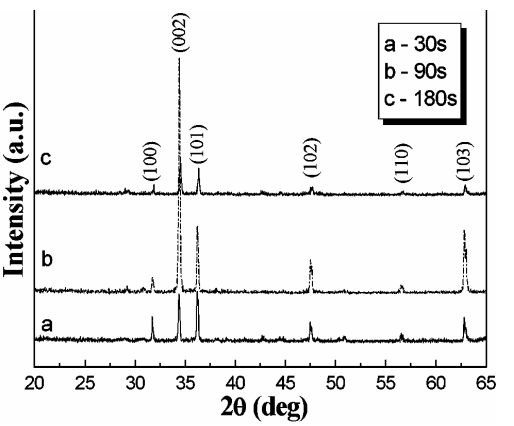

Fig. 3 XRD patterns of ZnO nanostructures synthesized with different given time of Ar.

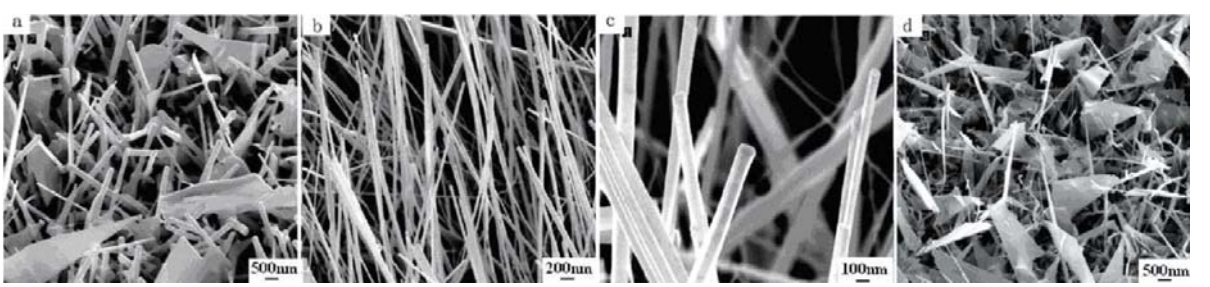

Fig. 2 SEM images of ZnO nanostructures grown with different given time of Ar: (a) 30 s, (b) and (c) 90 s, (d) 180 s.

3 Results and discussion

Figure 2 shows the scanning electron microscopy (SEM) images of three samples with different given time of Ar gas current. When the supply time of Ar is 30s, the sample shows the mixture of sheets and wires (Fig. 2a). The sheets are quadrate or triquetrous. The thickness is about 150 nm and the surfaces are smooth. The average diameter of wires is 200 nm. When the supply time increased to 90 s, the substrate was all covered with nanowires (Fig. 1b). Figure 2c shows the magnified view of the single nanowire, it can be seen that the tip behaves hexagonal shape. The average diameter of these ZnO nanowires is about 80 nm. The average ratio of length/diameter of the ZnO nanowires is estimated larger than 20. As figure 2d shows, with further increasing supply time of Ar to 180 s, big sheets appeared again. It can be also seen that some nanowires grow on these sheets. Therefore, different ZnO nanostructures were formed with the different supply time of the Ar gas in our experiments. Figure 3 shows the XRD patterns of the ZnO synthesized with the different supply time of Ar. No diffraction peaks of metallic Zn or other impurities can be observed besides ZnO peaks. The highest intensity

of (002) peak shows that those nanowires are well aligned along the c-axis. The intensity of the peak (002) significantly enhances with increasing given time of Ar to 90 s (Fig. 3b).

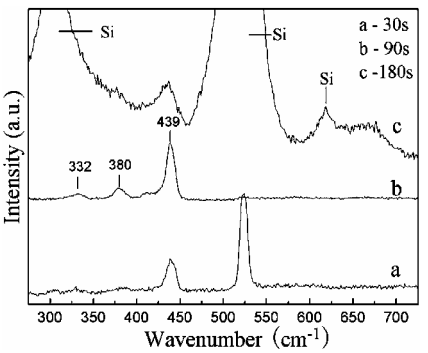

Fig. 4 Room temperature Raman spectra of ZnO synthesized with different supply time of Ar.

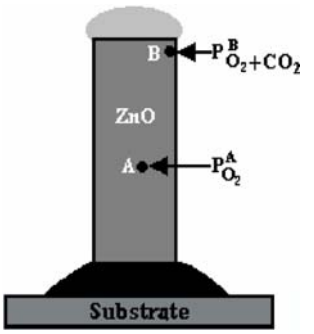

Fig. 5 Growth model of ZnO nanowires.

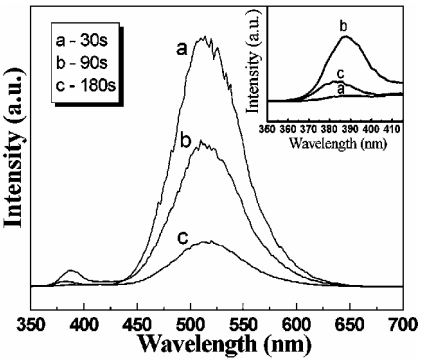

Fig. 6 Room temperature PL spectra of the ZnO nanostructures with different given time of Ar. The inset is the magnified view of UV emission region.

With increasing supply time of Ar to 180 s, the (002) peak declines evidently. High-temperature vapor phase growth has two mechanisms, including Vapor–liquid–solid mechanism [18] and Vapor–solid mechanism [19]. In our studies, ZnO growth is attributed to the VLS crystal growth mechanism. In this process, the supersaturation of alloy droplet plays an important role in the nucleation and growth process. ZnO is reduced by graphite firstly (at 900°C) to form Zn, and Zn (melting temperature is about 419°C) in the vapor phase is condensed to form liquid droplets on Si substrate as nuclear for ZnO nanowire growth. Then Zn in the liquid droplets is oxidized. Enhanced absorption and diffusion of ZnO occurred at the liquid tips. Eventually, ZnO super saturation results in ZnO segregation and nanowires array growth. The reaction process is shown as follows:

1. Reducing process:

$$ZnO_{(solid)} + C \rightarrow Zn_{(gas)} + CO_2$$

$$C + CO_2 \rightarrow 2CO_2$$

$$ZnO_{(solid)} + CO \rightarrow Zn_{(gas)} + CO_2$$

2. Oxidation process:

$$Zn_{(\text{dissolved in Au})} + CO_2 \rightarrow ZnO + CO$$

$$2Zn_{(\text{disslove in Au})} + O_2 \rightarrow 2ZnO$$

But it is also believed that oxygen in the system may be another important factor in the process. A schematic picture of the oxidation process is shown in figure 5. Point A denotes one place inside of ZnO nanowire, and point B denotes another place on surface of ZnO nanowires, their oxygen partial pressures are $p^{A}_{O_2}$ and $p^{B}_{O_2}$, respectively. O_2 must diffused through from outside to point A, so $p^{A}_{O_2}$ is smaller than $p^{B}_{O_2}$.We supposed that the difference between $p^{A}_{O_2}$ and $p^{B}_{O_2}$ might play an important role on the growth of ZnO nanowires. It can be concluded that there is a critic condition of $p^{A}_{O_2}$. At the beginning, the furnace is not sealed, so the argon flows into the furnace and the equal volume air would be run off. When finished supplying of Ar gas, air valves were closed at the same time. So the Ar gas can reduce the content of the oxygen in the furnace. In other words, the oxygen partial pressure is changed. If the supply time of the Ar was too long (180 s), the oxygen partial pressure was lower. At point B, the oxidation process can not carry out. ZnO will have bad quality. If the supply time of the Ar was too short, the carbon can be oxidized by oxygen and ZnO will not appear.

The space group of the hexagonal wurzite ZnO belongs to C_{6v}^{4}, with two formula units per primitive cell. According to the group theory, single-crystalline ZnO has eight sets of optical phonon modes at Γ point of the Brillouin zone, classified as $A_1+E_1+2E_2$ modes (Raman active), $2B_1$ modes (Raman silent), and A_1+E_1 modes (infrared active). Moreover, the A_1 and E_1 modes split into LO and TO components. As shown in figure 4, the peaks at 304, 521 and 620 cm^{-1} are Si vibration modes. The peaks at 332 [18], 380 [19] and 439 cm^{-1} [20] are

assigned to second-order Raman spectrum A_1 (E_2, E_1), A_{1T} and E_{2H}. The E_2 mode corresponds to bandcharacteristic of wurtzite phase [21,22]. Among of these samples, the E_2 mode of sample b has the stronger intensity and narrower line-width, which indicate that sample b is composed of ZnO with hexagonal wurtzite structure and good crystal quality. The E_{1L} mode at 578 cm^{-1} is due to the impurities and structural defects (oxygen vacancies and Zn interstitials [23]). The absence of the E_{1L} mode indicated that the as-grown products have low level of oxygen vacancies and Zn interstitials.

Figure 6 shows the room temperature PL spectra of samples a, b and c. The inset is UV spectra of the samples. All the PL spectra show an UV emission peak located at ~388nm (~3.2eV) and a broad, green emission peak dominated at ~520nm (~2.38eV). Sample b shows one relative strong UV emission compared with sample a and c, which indicate that it has relative good crystal quality [24] and it is consistent with results of XRD and Raman. The UV emission attributes to the near-band-edge emission, arises from the recombination of free excitons through an exciton-exciton collision process [25]. The excitonic luminescence may become suppressed due to increased defect concentration through trapping or non-radiative recombination at these defect centers [26]. So sample a and c have week UV emission. The green emission of ZnO is usually ascribed to structural defects, which included zinc vacancy (V_{Zn}), oxygen vacancy (V_O), interstitial zinc (Zn_i), interstitial oxygen (O_i) and antisite oxygen (O_{Zn}). It is believed that Oxygen vacancy (V_O) is the main reason of the green emission and the lower oxygen pressure the stronger the green emission. However, figure 6 shows that with the decline of oxygen pressure, the green emission become weak. Fu et al. [27] proposed the variation of these defects has direct relationship with the oxygen pressure (P_{O2}) during the growth process. Concentrations of V_O and Zn_i ought to increase with the decrease of the oxygen pressure (P_{O2}). On the contrary, concentrations of V_{Zn}, O_i and O_{Zn} should decrease with decrease of the P_{O2}. Therefore it is believe that the green emission should result from V_{Zn}, O_i and O_{Zn}. The energy interval from the bottom of the conduction band to V_{Zn}, O_i and O_{Zn} are 3.06 eV, 2.28 eV, and 2.38 eV, respectively. The energy of O_i and O_{Zn} defects approximately conform to the green emission in this work, but the probability of forming O_i is little due to the large diameter of oxygen atom. Therefore, the O_{Zn} should be responsible for the green band in our samples.

4 Conclusion

In summary, different Ar supply time at the beginning of the growth has effect on the morphologies. According to the analysis of PL spectra and experimental conditions, it is rather reasonable to believe that the green emission attributes to the electron transition from the bottom of the conduction band to the antisite defect O_{Zn} level.

Acknowledgements We would like to thank financial support of the program of National Natural Science Foundation of China (No. 60778040), State Key Program for Basic Research of China (No. 2003CD314702-02), the Science and Technology Bureau of Jilin Province (No. 20060518), Youth Program of Jilin Province (No. 20060123), Ministry of Education of China (No. 207025) and Education Bureau of Jilin Province (No. 2006111).

References

[1] Z. Pan, Z. Dai, and Z. L. Wang, Science **291**, 1947 (2001).
[2] D. Ma, C. Lee, F. Au, and S. T. Lee, Science **299**, 1874 (2003).
[3] X. Kong, Y. Ding, R. Yang, and Z. L. Wang, Science **303**, 1348 (2004).
[4] M. Huang, S. Mao, H. Fieck, H. Yan, Y. Wu, H. Kind, E. Weber, R. Russo, and P. Yang, Science **292**, 1897 (2001).
[5] H. Yan, R. He, J. Johnson, M. Law, R. Saykally, and P. Yang, J. Am. Chem. Soc. **125**, 4728 (2003).
[6] Gongping Li, Tao Chen, Bin Yan, Yun Ma, Zhou Zhang, Ting Yu, Zexing Shen, Hongyu Chen, and T. Wu, Appl. Phys. Lett. **92**, 173104 (2008).
[7] Q. Yu, B. Xu, Q. Wu, Y. Liao, G. Wang, R. Fang, H. Lee, and C. Lee, Appl. Phys. Lett. **83**, 4723 (2003).
[8] Z. Zhang, Y. H. Sun, Y. G. Zhao, G. P. Li, and T. Wu, Appl. Phys. Lett. **92**, 103113 (2008).
[9] R. H. Baughman, A. A. Zakhidov, and W. A. Hee, Science **297**, 787 (2002).
[10] J. Hu, T. W. Odom, and C. M. Lieber, Acc. Chem. Res. **32**, 435 (1999).
[11] J. R. Heath, P. J. Kuekes, G. Synder, and R. S. Williams, Science **280**, 1717 (1998).
[12] D. Snoke, Science **273**, 1351 (1996).
[13] M. Huang Y. Wu, H. Feick, N. Tran, E. Weber, and P. Yang, Adv. Mater. **13**, 113 (2001).

[14] D. M. Bagnall, Y. F. Chen, Z. Zhu, T. Yao, S. Koyama, M. Y. Shen, and T. Goto, Appl. Phys. Lett. **70**, 2230 (1997).
[15] H. Cao, J. Y. Xu, D. Z. Zhang, S. H. Chang, S. T. Ho, E. W. Seelig, X. Liu, and R. P. H. Chang, Phys. Rev. Lett. **84**, 5584 (2000).
[16] W. I. Park, D. H. Kim, S. W. Jung, and Gyu-Chui Yi, Appl. Phys. Lett. **80**, 4232 (2002).
[17] H. Kim and W. Sigmund, Appl. Phys. Lett. **81**, 2085 (2002).
[18] R. S. Wagner, W. C. Ellis, S. M. Arnold, and K. A. Jackson, J. Appl. Phys. **35**, 2993 (1964).
[19] Z. Zhang, S. J. Wang, T. Yu, and T. Wu, J. Phys. Chem. C **111**, 17500 (2007).
[20] J. M. Calleja and M. Cardona, Phys. Rev. B **16**, 3753 (1977).
[21] C. Arguello, D. Rousseau, and S. Porto, Phys. Rev. **181**, 1351 (1969).
[22] K. Alim, V. Fonoberov, and A. Balandin, Appl. Phys. Lett. **86**, 053103 (2005).
[23] G. J. Exarhos and S. V. Sharma, Thin Solid Films **270**, 27 (1995).
[24] Y. J. Xing, Z. H. Xi, Z. Q. Xue, X. D. Zhang, J. H. Song, R. M. Wang, J. Xu, Y. Song, S. L. Zhang, and D. P. Yu, Appl. Phys. Lett. **83**, 1689 (2003).
[25] K. Vanheusden, C. H. Seager, W. L. Warren, D. R. Tallant, and J. A. Voigt, J. Appl. Phys. **79**, 7983 (1996).
[26] F. Liu, P. J. Cao, H. R. Zhang, C. M. Shen, Z. Wang, J. Q. Li, and H. J. Gao, J. Cryst. Growth **274**, 126 (2005).
[27] Y. C. Kong, D. P. Yu, B. Zhang, W. Fang, and S. Q. Feng, Appl. Phys. Lett. **78**, 407 (2001).
[28] G. Xiong, U. Pal, J. G. Serrano, K. B. Ucer, and R. T. Williams, phys. stat. sol. (c) **3**, 3577 (2006).
[29] Bixia Lin, Zhuxi Fu, and Yunbo Jia, Appl. Phys. Lett. **79**, 943 (2001).

